IOP2021_2

by Leny Yuliati

Submission date: 27-Jul-2022 03:56PM (UTC+0800)
Submission ID: 1875757254
File name: y_of_Zinc_Metatitanate_Materials_for_Phenol_Photodegradation.pdf (980.71K)
Word count: 5186
Character count: 26061

High photocatalytic activity of zinc metatitanate materials for phenol photodegradation

High photocatalytic activity of zinc metatitanate materials for phenol photodegradation

K T A Priyangga[1], Y S Kurniawan[1] and L Yuliati[1,2,*]

[1]Ma Chung Research Center for Photosynthetic Pigments, Universitas Ma Chung, Malang 65151, Indonesia
[2]Department of Chemistry, Faculty of Science and Technology, Universitas Ma Chung, Malang 65151, Indonesia

*Email: leny.yuliati@machung.ac.id

Abstract. In this work, we synthesized zinc metatitanate ($ZnTiO_3$) through a sol-gel method strictly using a 1:1 mol ratio of zinc nitrate and titanium(IV) isopropoxide as the precursors. The calcination temperatures is set to 700, 900, and 1100 °C to give ZM-700, ZM-900, and ZM-1100, respectively. These ZM materials were characterized using X-ray diffractometer (XRD), diffuse reflectance ultraviolet-visible (DR UV-vis), Fourier transform infrared (FTIR), and fluorescence spectroscopies. The XRD analyses showed that the ZM-700 contained both cubic-$ZnTiO_3$ and rhombohedral-$ZnTiO_3$ phases with a small part of ZnO, while the ZM-900 contained cubic-$ZnTiO_3$ and cubic-Zn_2TiO_4. In contrast to the ZM-700 and the ZM-900, the ZM-1100 contained cubic-Zn_2TiO_4 and rutile TiO_2 as the main phases with a very small part of the $ZnTiO_3$ phase. The formation of these crystal phases was also supported by their DR UV-vis spectra, FTIR analysis, and fluorescence spectra. Photocatalytic degradation of phenol was carried out under UV light irradiation for 1–24 h. The kinetic study revealed that the reaction followed first-order, in which the reaction rate constants were 0.0351, 0.0323, 0.0298 h^{-1} for the ZM-700, ZM-900, and ZM-1100, respectively. This study demonstrated that the formation of $ZnTiO_3$ was crucial to obtain high photocatalytic activity on the ZM materials.

1. Introduction

Water pollution involving organic contaminants has gained significant attention due to its harmful effect on the environment. Phenol is considered as one of the organic pollutants present in the wastewater affecting the aquatic ecosystem [1]. The photocatalysis technique offers a promising way for the removal of this phenolic compound, in which it can degrade this contaminant to the less toxic compound of carbon dioxide (CO_2) and water (H_2O) [2]. Heterogeneous catalysts such as titanium dioxide (TiO_2)-based catalysts have been widely developed for this photocatalysis process [3-5]. Besides, binary metal oxide photocatalysts have also attracted great interest due to their excellent properties. These materials have been reported to exhibit good photocatalytic activity, such as the zinc titanates [6-10] and the zirconium titanates [11,12]. Particular attention is on the use of zinc titanate-based materials, which have been recognized as able to degrade organic pollutants.

Zinc titanates exist in different polymorphs, namely zinc metatitanate ($ZnTiO_3$), zinc orthotitanate (Zn_2TiO_4), and meta-stable zinc titanate ($Zn_2Ti_3O_8$). While the $ZnTiO_3$ has two different crystal phases of cubic (c-$ZnTiO_3$) and rhombohedral (r-$ZnTiO_3$) [13,14], the Zn_2TiO_4 is found in cubic crystal phase (c-

Zn_2TiO_4) or cubic with inverse spinel structure, and $Zn_2Ti_3O_8$ is only available in cubic phase (c-$Zn_2Ti_3O_8$) [15,16]. These polymorphs have been also used to increase the activity of other metal oxide photocatalysts, such as in the $ZnTiO_3$/$Zn_2Ti_3O_8$/ZnO [6] and g-C_3N_4/c-$ZnTiO_3$/TiO_2 [17]. The $ZnTiO_3$/$Zn_2Ti_3O_8$/ZnO was used for the degradation of Rhodamine B and the reduction of Cr(VI) [6], while the g-C_3N_4/c-$ZnTiO_3$/TiO_2 was used to degrade methylene blue [17]. In both cases, the $ZnTiO_3$ phase was proposed to be responsible for the photocatalytic activity enhancement of the materials [6,17].

In order to obtain zinc titanates with the desired polymorph and crystal phase, the stoichiometric mol ratio of Zn and Ti as well as the synthesis temperature are the pivotal parameters [18,19]. The $ZnTiO_3$ could be synthesized when the mol ratio of Zn and Ti was 1:1 and at a certain temperature [20,21]. When the $ZnTiO_3$ was prepared by a precipitation method, the temperature of 600 °C was crucial as below the temperature the $Zn_2Ti_3O_8$ was formed as the main crystal phase [20]. Using the hydrothermal method, the $ZnTiO_3$ could be formed at the calcination temperature range of 600–900 °C [21]. However, the preparation of pure $ZnTiO_3$ was quite difficult because the ZnO was also co-existed in the prepared material. In the present study, we employed a sol-gel method to synthesize the $ZnTiO_3$ at various calcination temperatures (700, 900, and 1100 °C). The effects of the calcination temperature on the formation of polymorphs zinc titanates, their properties, and their photocatalytic activity for phenol degradation under UV light irradiation were examined.

2. Experimental Section

2.1. General

The materials used in this work were titanium(IV) isopropoxide (TTIP, $Ti(OC_3H_7)_4$, 97%), zinc nitrate hexahydrate ($Zn(NO_3)_2{\cdot}6H_2O$, 98%), sodium hydroxide (NaOH, 99%), ethanol (C_2H_5OH, > 99.9%), and phenol (C_6H_5OH, 99%). All the materials were purchased from Merck and used without any further purifications.

The instrumentations used this work were powder X-ray diffractometer (XRD, Rigaku SmartLab, PhotonMax high-flux 9 kW), ultraviolet-visible spectrophotometer (UV-vis, JASCO V-760) attached with an integrating sphere (ISV-922/ISN-923/ISN-901i), Fourier transform infrared spectroscopy (FTIR, JASCO 6800) attached with an attenuated total reflectance (ATR, Pro One), and fluorescence spectrophotometer (JASCO FP-8500). High-performance liquid chromatography (HPLC, Shimadzu LC-20 AT) with a photodiode array detector (PDA, SPD-M20) was used for phenol analysis at 272 nm. The stationary and mobile phase used in the HPLC were a C18 column and 100% acetonitrile, respectively. The column temperature was set to 40 °C and the flow rate was set to 0.8 mL min^{-1}.

2.2. Procedure

2.2.1. Synthesis of ZM materials. The $ZnTiO_3$ was prepared by a sol-gel method, followed by the calcination process at different temperatures to give zinc metatitanate (ZM) materials. In a typical preparation method, the TTIP (3.50 g, 0.0123 mol) was dissolved in ethanol (10 mL) to produce solution A, while the $Zn(NO_3)_2{\cdot}6H_2O$ (3.65 g, 0.0123 mol) was dissolved with ethanol (10 mL) to produce solution B. Solution B was then poured into solution A, followed by a dropwise addition of NaOH (1 M, 2 mL) into the mixture. The mixture was kept stirred at room temperature for 1 hour to homogenize the mixture. The solvent was evaporated slowly by heating the mixture at 60 °C for 24 hours to allow sol-gel formation. The white solid was ground into a powder and calcined at different temperatures of 700, 900, and 1100 °C for 6 hours to give ZM-700, ZM-900, and ZM-1100, respectively.

2.2.2. Characterization of ZM materials. The ZM materials were characterized by XRD to identify their crystal phases. The diffractogram was measured at room temperature in the 2θ range of 20–80 degrees. The diffuse reflectance UV-visible (DR UV-vis) spectrum of each sample was collected on a UV-vis spectrophotometer, in which the measurement was made in the range of 200–800 nm and shown as

Kubelka-Munk (KM) function. The FTIR spectra were recorded by the ATR method at the wavenumber range of 4000–400 cm^{-1}. The emission and excitation fluorescence spectra of each sample were recorded at room temperature with an emission wavelength ($\lambda_{emission}$) of 302 nm and an excitation wavelength ($\lambda_{excitation}$) of 274 nm [3].

2.2.3. *Photocatalytic Phenol Degradation on ZM Materials*. The ZM materials were evaluated for photocatalytic degradation of phenol under UV light irradiation at room temperature. An aqueous phenol solution (50 mg L^{-1}, 50 mL) was used for such a purpose. The ZM sample (50 mg) was added into the phenol solution and stirred for 2 hours in the dark condition to reach the adsorption equilibrium. The reaction was then started by illuminating the mixture using a UV lamp (UVLS-28 EL Series, 365 nm, 8 W) for 1, 3, 6, 15, and 24 hours. After the illumination, the mixture was filtered and then the phenol concentration in the filtrate was analyzed by the HPLC. The photocatalytic activity was determined from the percentage of phenol degradation, which was calculated from the ratio of decreased phenol concentration after reaction (C_0 - C_t) to the initial phenol concentration (C_0) as shown in equation (1). C_t is phenol concentration after a certain time of reaction.

$$\text{Photodegradation } (\%) = \frac{(C_0 - C_t)}{C_0} \times 100\% \quad (1)$$

3. Results and discussion

3.1. *Physicochemical Properties of ZM Materials*

The XRD pattern was analyzed to identify the crystal phases present on each material calcined at different temperatures of 700, 900, and 1100 °C. As shown in Figure 1, the synthesized ZM materials have various crystal phases, which could be indexed to c-$ZnTiO_3$ (JCPDS 00-039-0190) [22], r-$ZnTiO_3$ (JCPDS 00-026-1500) [13,23], ZnO (JCPDS 00-036-1451) [22], c-Zn_2TiO_4 (JCPDS 00-073-0578) [22], c-Zn_2TiO_4 inverse-spinel (JCPDS 00-025-1164) [15], and rutile TiO_2 or r-TiO_2 (JCPDS 00-021-1276) [15].

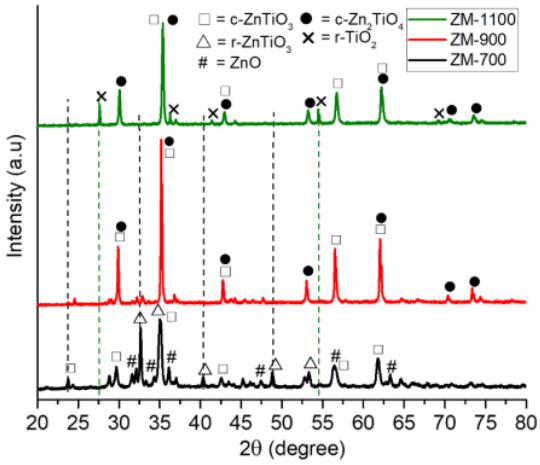

Figure 1. XRD patterns of ZM materials.

The ZM-700 consisted of c-$ZnTiO_3$ and r-$ZnTiO_3$, as well as the ZnO phase. The formed crystal phase was affected by the synthesis temperature. When the synthesis was carried out at a higher temperature of

900 °C, the diffraction peaks of the c-$ZnTiO_3$ still could be observed, however, the diffraction peaks of r-$ZnTiO_3$ were diminished and the ZnO peaks were decreased in intensity. In addition to the c-$ZnTiO_3$, the c-Zn_2TiO_4 peaks were also observed in the ZM-900. This result showed that at 900 °C the r-$ZnTiO_3$ could be transformed into the c-$ZnTiO_3$ and the r-$ZnTiO_3$ could react with ZnO to produce the c-Zn_2TiO_4 as depicted in equation (2). In contrast to the ZM-700 and the ZM-900, the ZM-1100 not only contained c-$ZnTiO_3$ and c-Zn_2TiO_4, but also contained r-TiO_2. The formation of r-TiO_2 was possible since the c-$ZnTiO_3$ could be decomposed to c-Zn_2TiO_4 and r-TiO_2 at 1100 °C [24,25] as shown in equation (3). It was worthy to note that the formation of the c-$ZnTiO_3$ was further reduced with the increase of the calcination temperature.

$$ZnO\ (s) + r\text{-}ZnTiO_3\ (s) \rightarrow c\text{-}Zn_2TiO_4\ (s) \quad (2)$$

$$2\ c\text{-}ZnTiO_3\ (s) \rightarrow c\text{-}Zn_2TiO_4\ (s) + r\text{-}TiO_2\ (s) \quad (3)$$

The DR UV-vis spectra of the ZM materials were also recorded to study their optical properties. The plots of Kubelka-Munk (KM) function versus wavelength for all the ZM materials are shown as DR UV-vis spectra in Figure 2(a). Different calcination temperatures resulted in the different absorption properties of the ZM materials. The ZM-700 showed several absorption peaks at 219, 257, and 297 nm, while the ZM-900 exhibited absorption peaks at 221, 257, and 311 nm. In addition, the ZM-700 gave the characteristic absorption of ZnO, giving an absorption edge close to 390 nm. The shifted absorption peak from 297 to 311 nm with the increase of the calcination temperature from 700 to 900 °C would be related to the additional formation of c-Zn_2TiO_4 as suggested by the XRD pattern. The ZM-1100 gave absorption peaks at 254, 303, and 390 nm. The first and second absorption peaks could be assigned to the c-$ZnTiO_3$ and c-Zn_2TiO_4, while the latter would be due to the presence of the r-TiO_2, as supported by its XRD pattern.

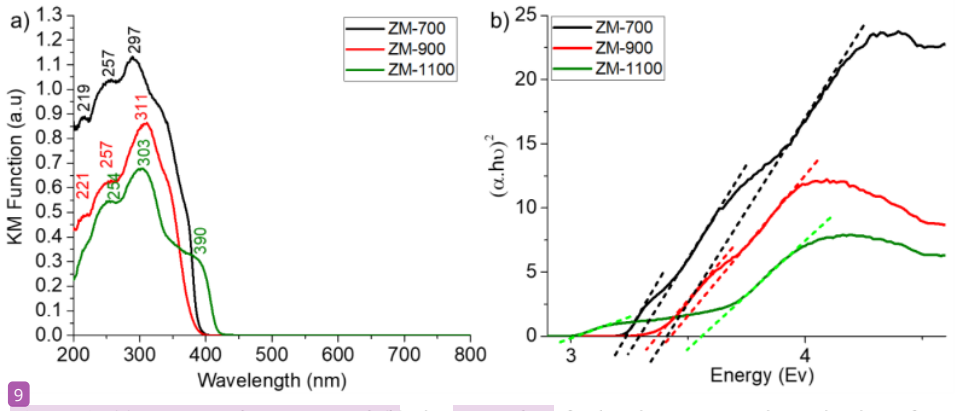

Figure 2. (a) DR UV-vis spectra and (b) the Tauc plots for bandgap energy determination of ZM materials.

Bandgap energy is an important parameter related to photocatalytic activity. The bandgap energy value determines the minimum energy required to excite electrons from the valence band to the conduction band of a photocatalyst material. The bandgap energy values of the ZM-materials were determined using the Tauc method with a direct bandgap manner as shown in equation (4) [26]. The bandgap energy is symbolized as *Eg*, while the α, *h*, and υ are referring to the absorption coefficient related to the material, Plack constant, and light frequency, respectively.

$$(ah\upsilon)^2 = A\left(E_g - h\upsilon\right) \quad (4)$$

The extrapolation of the linear plot between the $(\alpha h\upsilon)^2$ versus $(h\upsilon)$ to the x-axis can be used to determine bandgap energy value of each material. The Tauc plot of the ZM-700, the ZM-900, and the ZM-1100 are shown in Figure 2(b) and the bandgap energy values are summarized in Table 1. It could be observed that ZM materials have multiple bandgap energies. The bandgap energy values of ZM-700 were determined to be 3.36, 3.28, and 3.23 eV, which could be correlated to the presence of the c-ZnTiO$_3$, r-ZnTiO$_3$, and ZnO respectively [27,28]. The ZM-900 has two distinguished bandgap energy values of 3.36 and 3.44 eV, which could be assigned to the c-ZnTiO$_3$ and the c-Zn$_2$TiO$_4$. In contrast to the ZM-700 and ZM-900, the ZM-1100 did not show the characteristic bandgap value of c-ZnTiO$_3$. The ZM-1100 has bandgap energy values of 3.56 eV due to the presence of c-Zn$_2$TiO$_4$ and 3.02 eV from the r-TiO$_2$ [29,30]. This result was also in agreement with the XRD pattern, in which the ZM-1100 contained the c-Zn$_2$TiO$_4$ and r-TiO$_2$ as the main crystal phase with c-ZnTiO$_3$ as the minor phase.

Table 1. Bandgap values of the ZM materials.

Materials	Bandgap energy (eV)	Assignment [27-30]
ZM-700	3.36	c-ZnTiO$_3$
	3.28	r-ZnTiO$_3$
	3.23	ZnO
ZM-900	3.36	c-ZnTiO$_3$
	3.44	c-Zn$_2$TiO$_4$
ZM-1100	3.56	c-Zn$_2$TiO$_4$
	3.02	r-TiO$_2$

The FTIR spectra of the ZM materials were analyzed to identify the functional vibrational modes present in each sample. As depicted in Figure 3(a), all the ZM materials exhibited no O–H vibrational stretching mode (3400 cm^{-1}) of adsorbed water molecules [31]. This could be caused by the employed high calcination temperature in the synthesis process. On the other hand, all ZM-materials showed peak absorption peaks in the range of 883–970, 693–699, 639–641, 546–548, 490–506, and 400–430 cm^{-1} as shown in Figure 3(b). The strong broad absorption band at 883–970 cm^{-1} could be related to the vibrational mode of Ti–O stretching, involving non-bridging oxygen atoms. In the ZM-900 and the ZM-1100, the intensity of this band was decreased and also shifted to the higher wavenumber. This change could be ascribed as the indication of crystal phase transformation of the ZM materials with the increase in the calcination temperature [32], as also confirmed from the XRD results. The Zn–O–Ti vibrational mode was observed as a shoulder band in the region of 693–699 cm^{-1}, which was the characteristic of zinc titanate materials [33]. The other bands in the region of 639–641 cm^{-1} and 400–430 cm^{-1} were related to the vibrational mode of Ti-O bending in $[TiO_6]^{2-}$ octahedral in the ZM materials [6]. In addition, the broad band in the region of 700 cm^{-1} was assigned to be the vibrational mode of O–Ti–O stretching in $[TiO_6]^{2-}$ octahedral, which was in good agreement with the reported literature [34]. On the other side, the presence of $[ZnO_4]^{2-}$ structure in ZM materials was also observed as a shoulder band in the region of 546–548 cm^{-1} and 490–506 cm^{-1}, which was related to the vibrational mode of Zn–O bending [35,36]. The most intense peak at 506 cm^{-1} in the ZM-700 as compared to those of the ZM-900 and ZM-1100 would be related to the presence of the ZnO crystal phase in this ZM-700 as confirmed from the XRD result.

Fluorescence properties of the ZM-700, ZM-900, and ZM-1100 materials are depicted in Figure 4. As shown in Figure 4(a), all the ZM materials gave a similar shape of excitation spectrum to each other. The excitation peak was observed at 274 nm when 302 nm was used as the emission wavelength. The increase in the calcination temperature increased the excitation intensity. The excitation intensity of the ZM-700 was still close to that of the ZM-900, but lower than that of the ZM-1100. The emission spectra of the ZM materials were monitored at the excitation wavelength of 274 nm and shown in Figure 4(b). All the ZM

materials gave a similar main emission peak at 302 nm and slightly different shapes of low emission peaks at 360–700 nm. As expected from their excitation intensity, the ZM-700 and the ZM-900 showed similar emission intensity, while the ZM-1100 gave much higher emission intensity. The emission intensity could be ascribed to the recombination of trapped electron-hole [3] at the different energy levels of the ZM-materials. The difference between the ZM-700 and the ZM-900 as compared to the ZM-1100 could be also observed from the emission fine structure at the visible region. Such differences could be correlated to the different main crystal phases in these ZM materials as previously discussed from the XRD patterns and DR UV-vis spectra.

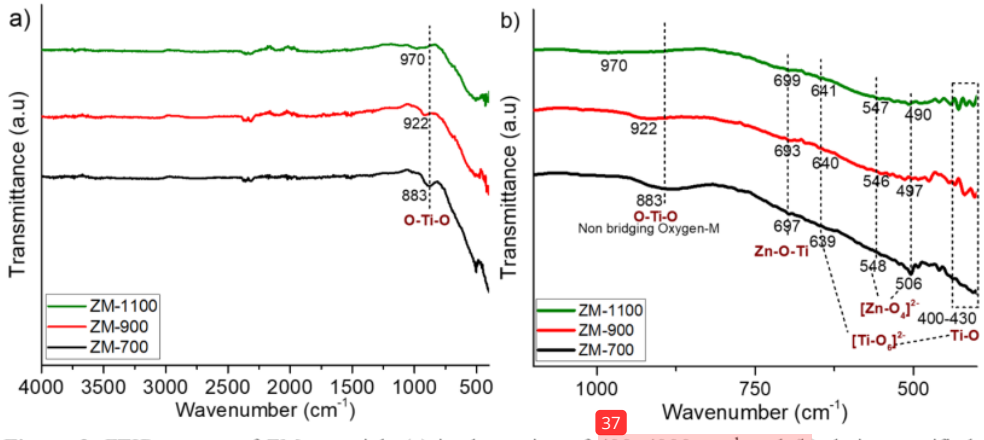

Figure 3. FTIR spectra of ZM materials (a) in the region of 400–4000 cm^{-1} and (b) their magnified spectra in the region of 400–1100 cm^{-1}.

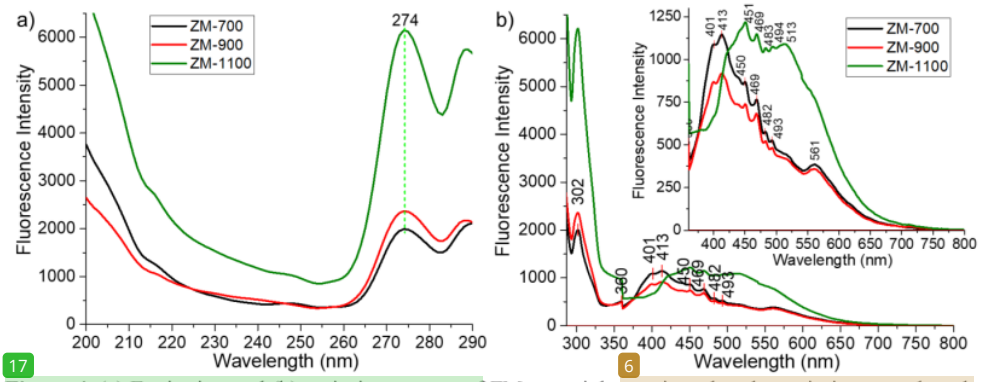

Figure 4. (a) Excitation and (b) emission spectra of ZM materials monitored at the emission wavelength of 302 nm and excitation wavelength of 274 nm, respectively. Inset shows the magnified emission spectra at 360–800 nm.

3.2. *Photocatalytic activity of ZM materials*

The photocatalytic activity of each ZM-700, ZM-900, and ZM-1100 materials was evaluated for the degradation of phenol under UV light. Figure 5(a) shows the plot between the ratio of phenol concentration at a certain reaction time (C_t) to the initial phenol concentration (C_0) versus the reaction time (t). The ZM-700 gave the highest photocatalytic activity followed by ZM-900, and the ZM-1100. After 24 hours, the phenol degradation percentage for the ZM-700, ZM-900, and ZM-1100 were 57, 56, and 50%, respectively. The difference in the photocatalytic activity could be affected by the different crystal phases present in the ZM materials. The ZM-700 having the c-$ZnTiO_3$ and r-$ZnTiO_3$ as the main crystal phases gave the highest activity. The ZM-900 also has c-$ZnTiO_3$ and thus, a similar level of activity to the ZM-700 was also observed. The slightly decreased activity could be due to the less active c-Zn_2TiO_4 in this ZM-900. The decreased activity was more observed on the ZM-1100 having c-Zn_2TiO_4 and r-TiO_2 as the main crystal phases with the c-$ZnTiO_3$ as the minor phase. Therefore, the presence of r-TiO_2 could be also the reason for the decreased activity. Besides, as shown in the fluorescence study, the ZM-1100 gave a high emission intensity, which could be the result of the high electron-hole recombination process. All these results demonstrated that both c-$ZnTiO_3$ and r-$ZnTiO_3$ were the ones corresponding to the high photocatalytic activity of the ZM materials.

The kinetic photocatalytic activity of the ZM materials for the photodegradation of phenol was evaluated using equation (5). The reaction rate constant (k) for each ZM material was calculated from the slope of the linear plots between the $-\ln(C_t/C_0)$ and the reaction time (t).

$$-\ln\left(\frac{C_t}{C_0}\right) = kt \quad (5)$$

As shown in Figure 5(b), it was clarified that all the reactions over the ZM materials followed the first-order reaction kinetic model as usually proposed for the photocatalytic degradation reaction [37]. The degradation rate constants for the ZM-700, the ZM-900, and the ZM-1100 were determined to be 0.0351, 0.0323, and 0.0298 h^{-1}, respectively. This result again confirmed that the presence of $ZnTiO_3$ would be important to give high activity for phenol degradation.

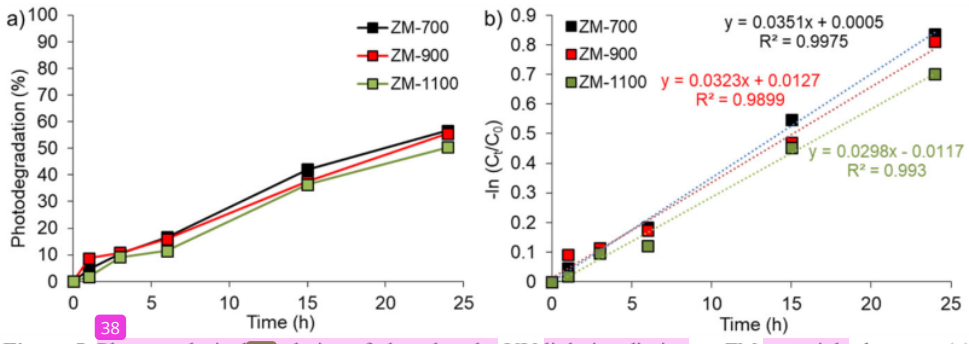

Figure 5. Photocatalytic degradation of phenol under UV light irradiation on ZM materials shown as (a) plots of photodegradation percentage versus time and (b) plots of -ln (C_t/C_0) versus time.

Since the reported conditions for photocatalytic degradation of phenol involved various parameters, the activity comparison between the ZM-700 and other reported $ZnTiO_3$ photocatalysts [6,31,38] could be determined from the turn over frequency (TOF) values. Considering that the $ZnTiO_3$ was proposed as the main active sites for the phenol degradation, the TOF values could be calculated from equation (6), where the amount of the active sites was determined solely from the amount of photocatalyst.

$$TOF = \frac{\text{amount of converted phenol}}{\text{amount of active sites} \times \text{reaction time}} \quad (6)$$

Unfortunately, the real amount of $ZnTiO_3$ existing in the ZM-700 was not examined in this study. Judging from the absorbance intensity, the ratio of the $ZnTiO_3$ intensity to the ZnO intensity was close to 70%. Taking into account an assumption if the ZM-700 consisted of $ZnTiO_3$ phase in the range of 70–100%, the TOF value would be in the range of 2.04×10^{-3}–2.91×10^{-3} h^{-1}. As listed in Table 2, this value was still at a similar level to the TOF values calculated from the reported data on $ZnTiO_3$ photocatalysts prepared by other methods, which was in the range of 3.29×10^{-3}–3.73×10^{-3} h^{-1}. The similar level suggested that the similar active sites, which were the $ZnTiO_3$, were involved in the reaction. The slightly lower TOF value of the ZM-700 would be due to other parameters, such as the use of different light sources which would lead to different light intensity. The reaction in this study was carried out under an 8 W UV lamp, while all the reported reactions were conducted under irradiation of strong UV lamp power (400–500 W) [6,31,38].

Table 2. Activity comparison of $ZnTiO_3$-based photocatalysts for phenol degradation.

Materials	Preparation method (temperature)	Reaction conditions	Photodegradation (%)	TOF (10^{-3} h^{-1})
ZM-700	Sol-gel (700 °C)	Photocatalyst (50 mg), phenol (50 mg L^{-1}, 50 mL), irradiation time (24 h), UV lamp (8 W)	57	2.04 – 2.91[a]
$ZnTiO_3$ [6]	Solvothermal (700 °C)	Photocatalyst (50 mg), phenol (10 mg L^{-1}, 80 mL), irradiation time (2.5 h), UV lamp (500 W)	30	3.29
$ZnTiO_3$ [31]	Solvothermal (700 °C)	Photocatalyst (50 mg), phenol (10 mg L^{-1}, 80 mL), irradiation time (2.5 h), UV lamp (400 W)	34	3.73
$ZnTiO_3$ [38]	No information[b]	Photocatalyst (100 mg), phenol (25 mg L^{-1}, 200 mL), irradiation time (2.5 h), UV lamp (500 W)	10	3.43

[a]Based on the rough assumption of $ZnTiO_3$ content in ZM-700 (70–100%).
[b]Commercially available from Sigma-Aldrich.

The proposed mechanism of photocatalytic phenol degradation on the ZM-700 is displayed in Figure 6. The valence band positions of $ZnTiO_3$ and ZnO were also shown according to the reported values [39]. In general, it is well-known that the metal oxide materials act as a photocatalyst since they can generate the pair of excited electrons and holes during the UV light irradiation process. In this work, the ZM materials were confirmed to have multiple bandgap energy since the ZM materials consisted of several semiconductors. For instance, the ZM-700 was shown to have c-$ZnTiO_3$, r-$ZnTiO_3$, and ZnO phases. Therefore, electron excitations would occur on all these semiconductors if the light source has energy higher than their bandgap energy. Since a UV lamp of 365 nm (3.4 eV) was employed in this work, the electron excitation could occur on c-$ZnTiO_3$ (3.36 eV), r-$ZnTiO_3$ (3.28 eV), and ZnO (3.23 eV) phases. As shown in Figure 6, the excited electrons could reduce the dissolved oxygen to create superoxide radicals that would further oxidize phenol to carbon dioxide and water. On the other hand, the remaining holes would react with water to form hydroxyl radicals which are strong enough to oxidize phenol. In addition, since the conduction band position of $ZnTiO_3$ is slightly more negative than that of the ZnO, the possibility that electron transfers also occur from the conduction band of the $ZnTiO_3$ to the conduction

band of the ZnO could not be neglected. The charge transfer could also proceed between the $ZnTiO_3$ phases. A further study shall be carried out to clarify the detailed charge transfer pathways in the ZM materials.

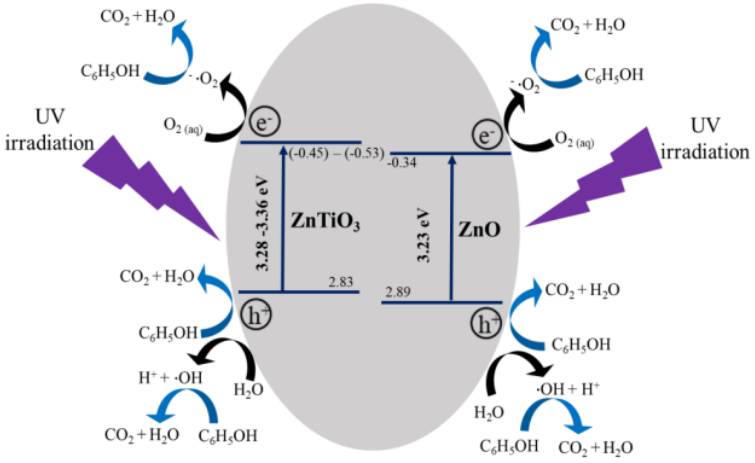

Figure 6. Proposed mechanism of photocatalytic phenol degradation on the ZM-700.

4. Conclusions

The ZM materials were successfully synthesized by the sol-gel method using titanium(IV) isopropoxide and zinc(II) nitrate as the precursors with 1:1 mol ratio. Different calcination temperatures (700, 900, 1100 °C) were revealed to affect the formation of different crystal phases in the ZM materials. As confirmed from the XRD patterns, the $ZnTiO_3$ crystal phase was mainly formed in the ZM-700 and the ZM-900 but not in the ZM-1100. Similar optical properties of the ZM-700 and the ZM-900 were also confirmed from the DR UV-vis, FTIR, and fluorescence spectroscopies analyses. In contrast, the ZM-1100 contained c-Zn_2TiO_4 and r-TiO_2 as the main crystal phases as the result of the decomposition of $ZnTiO_3$ at the high temperature. All the photocatalytic degradation phenol over the ZM materials followed the first-order kinetic reaction. The degradation rate constants for the ZM-700, the ZM-900, and the ZM-1100 were 0.0351, 0.0323, and 0.0298 h^{-1}, respectively. Both the c-$ZnTiO_3$ and the r-$ZnTiO_3$ crystal phases in ZM materials were proposed as the main active phases for the photocatalytic degradation of phenol.

References

[1] Michałowicz J and Duda W 2007 *Pol. J. Environ. Stud.* **16** 347.
[2] Ahmed S, Rasul M G, Martens W N, Brown R and Hashib M A 2011 *Water Air Soil Pollut.* **215** 3
[3] Mathew S, Kumar Prasad A, Benoy T, Rakesh P P, Hari M, Libish T M and Vallabhan C P G 2012 *J. Fluoresc.* **22** 1563.
[4] Ahmed S, Rasul M G, Martens W N, Brown R and Hashib M A 2010 *Desalin.* **261** 3.
[5] Choquette-Labbé, M, Shewa W A, Lalman J A and Shanmugam S R 2014 *Water* **6** 1785.
[6] Chen F, Yu C, Wei L, Fan Q, Ma F, Zeng J and Ji H 2019 *Sci. Total Environ.* **706** 136026.
[7] Hong Z, Wei M, Deng Q, Ding X, Jiang L and Wei K 2010 *Chem. Commun.* **46** 740.
[8] Qu Y, Zhou W, Ren Z, Wang G, Jiang B and Fu H 2014 *Chem. Cat. Chem.* **6** 2258.
[9] Zhao M, Bastakoti B P, Li, Y, Xu H, Ye J, Liu Z and Yamauchi Y 2015 *Chem. Commun.* **51** 14582.
[10] Sutanto N, Saharudin K A, Sreekantan S, Kumaravel V and Akil H M 2019 *J. Sol-Gel Sci. Technol.*

93 354.
[11] Badli N A, Ali R, Bakar W A W A and Yuliati L 2017 *Arab. J. Chem.* **10** 935.
[12] Andita K R, Kurniawan R and Syoufian A 2019 *Indones. J. Chem.* **19** 761.
[13] Tian H, Wang S, Zhang C, Veder J P, Pan J, Jaroniec M and Liu J 2017 *J. Mater. Chem. A.* **5** 11615.
[14] Wang L, Kang H, Xue D and Liu C 2009 *J. Cryst. Growth* **311** 611.
[15] Lokesh B and Rao N M 2016 *J. Mater. Sci. Mater. Electron.* **27** 4253.
[16] Arin J, Thongtem S, Phuruangrat A and Thongtem T 2017 *Mater. Lett.* **193** 270.
[17] Li X, Xiong J, Huang J, Feng Z and Luo J 2019 *J. Alloys Compd.***774** 768.
[18] Budigi L, Nasina M R, Shaik K and Amaravadi S 2015 *J. Chem. Sci.* **127** 509.
[19] Wang C L, Hwang W S, Chang K M, Co H H, Hsi C S, Huang H H and Wang M C 2011 *Int. J. Mol. Sci.* **12** 935.
[20] Chang Y S, Chang Y H, Chen I G, Chen G J, Chai Y L, Fang T H and Wu S 2004 *Ceramics Int.* **30** 2183.
[21] Jose M, Elakiya M and Dhas S A M B 2017 *J. Mater. Sci. Mater. Electron.* **28** 13649.
[22] Lokesh B, Madhusudhana Rao N, Kaleemulla S and Sivakumar A 2015 *Chemical Papers* **69** 1.
[23] Arin J, Thongtem S, Phuruangrat A and Thongtem T 2016 *Res. Chem. Intermed.* **43** 3183.
[24] Eskandarloo H, Badiei A, Behnajady M A, Tavakoli A and Ziarani G M 2016 *Ultrason. Sonochem.* **29** 258.
[25] Mrázek J, Spanhel L, Chadeyron G and Matějec V 2010 *J. Phys. Chem. C* **114** 2843.
[26] Viezbicke B D, Patel S, Davis B E and Birnie D P 2015 *Phys. Status Solidi B* **252** 1700.
[27] Mullerova J, Sutta P, Medlin R, Netrvalova M, Novak P 2017 *J. Electr. Eng.* **68** 10.
[28] Davis K, Yarbrough R, Froeschle M, White J and Rathnayake H 2019 *RSC Advances* **9** 14638.
[29] Mebrek A, Alleg S, Benayache S and Benabdeslem M 2018 *Ceram. Int.* **44** 10921.
[30] García-Ramírez E, Mondragón-Chaparro M and Zelaya-Angel O 2012 *Appl. Phys. A* **108** 291.
[31] Yu C, Chen F, Zhou W, Xie Y, Zeng D, Liu Z, Wei L, Yang K and Li D 2019 *Nanoscale* **11** 7720.
[32] Babu B C, Naresh V, Prakash B J and Buddhudu S 2011 *Ferroelectr. Lett. Sect.* **38** 114.
[33] Wang J X, Huang J, Xie H L and Qu A L 2014 *Int. J. Hydrog. Energ.* **39** 6354.
[34] Mohammadi M R and Fray D J 2010 *J. Eur. Ceram. Soc.* **30** 947.
[35] Liu G, Li G, Qiu X and Li L 2009 *J. Alloys Compd.* **481** 492.
[36] Musić S, Popović S, Maljković M and Dragčević Đ 2002 *J. Alloys Compd.* **347** 324.
[37] Nickeslat A, Amin M M, Izanloo H, Fatehizadeh A and Mousavi S M 2013 *J. Environ. Public Health* **815310** 1.
[38] Zhou G, Sun H, Wang S, Ang H M and Tadé M O 2011 *Sep. Purif. Technol.* **80** 626.
[39] Lei S, Fan H, Ren X, Fang J, Ma L and Liu Z 2017 *J. Mater. Chem. C* **5** 4040.

Acknowledgements
This research was financially supported by the Directorate General of Strengthening Research and Development, Ministry of Research, Technology, and Higher Education of the Republic of Indonesia through the Higher Education Excellent Applied Research Grant (PTUPT 2020, No. 041/SP2H/AMD/LT/MULTI/L7/2020 and No. 002/MACHUNG/LPPM/SP2H-LIT-MULTI/AMD/VI/2020).

IOP2021_2

ORIGINALITY REPORT

20%	15%	18%	2%
SIMILARITY INDEX	INTERNET SOURCES	PUBLICATIONS	STUDENT PAPERS

PRIMARY SOURCES

1	Hary Devianto, Isdiriyani Nurdin, Pramujo Widiatmoko, Kafi Adi Prasetya, Basil Pradipta. "Effects of Fe-Doped Electrolyte and Feed Flow Rate Evaluation in Home Made Solid Oxide Fuel Cell", IOP Conference Series: Materials Science and Engineering, 2021 Publication	5%
2	Y S Kurniawan, K Anggraeni, R Indrawati, L Yuliati. "Functionalization of titanium dioxide through dye-sensitizing method utilizing red amaranth extract for phenol photodegradation", IOP Conference Series: Materials Science and Engineering, 2020 Publication	1%
3	mafiadoc.com Internet Source	1%
4	K T A Priyangga, Y S Kurniawan, L Yuliati. "Synthesis and characterizations of C-3-Nitrophenylcalix[4]resorcinarene as a potential chemosensor for La(III) ions", IOP	1%

	Conference Series: Materials Science and Engineering, 2020 Publication	
5	www.science.gov Internet Source	1 %
6	Christyowati Primi Sagita, Leny Yuliati. "Photocatalytic degradation of phenol over carbon nitrides prepared by urea and melamine precursors", AIP Publishing, 2021 Publication	1 %
7	www.mdpi.com Internet Source	1 %
8	iopscience.iop.org Internet Source	1 %
9	Leny Yuliati, Mohd Hayrie Mohd Hatta, Siew Ling Lee, Hendrik O. Lintang. "Crystalline carbon nitride for photocatalytic phenol degradation: Effect of precursor and salt melt amounts", AIP Publishing, 2020 Publication	1 %
10	link.springer.com Internet Source	1 %
11	Peggy Tiong, Hendrik O. Lintang, Salasiah Endud, Leny Yuliati. "Reduced Graphene Oxide-Mesoporous Carbon Nitride as Photocatalyst for Removal of N-	1 %

Nitrosopyrrolidine", Advanced Materials Research, 2015
Publication

12	doaj.org Internet Source	<1 %
13	Leny Yuliati, Nor Shuhada Alim, Hendrik O. Lintang. "Improving the activity of rutile titanium dioxide with reduced graphene oxide", AIP Publishing, 2017 Publication	<1 %
14	ejournal.mrcpp.machung.ac.id Internet Source	<1 %
15	aip.scitation.org Internet Source	<1 %
16	Kazi Hasibur Rahman, Asit Kumar Kar. "Hydroxylation induced defect states and formation of bidentate acetate adstructure of TiO2 catalysts with acetic acid variation for catalytic application", Semiconductor Science and Technology, 2022 Publication	<1 %
17	Wynona A. Nimpoeno, Hendrik O. Lintang, Leny Yuliati. "Methyl red dye-sensitized zinc oxide as photocatalyst for phenol degradation under visible light", AIP Publishing, 2020 Publication	<1 %

18	F U Ermawati, N A Imamah. " Study on Heating Profile of Liquid-mixing-synthesized ZnTiO ", IOP Conference Series: Materials Science and Engineering, 2019 Publication	<1 %
19	Www.mdpi.com Internet Source	<1 %
20	Wynona A. Nimpoeno, Hendrik O. Lintang, Leny Yuliati. "Zinc Oxide with Visible Light Photocatalytic Activity Originated from Oxygen Vacancy Defects", IOP Conference Series: Materials Science and Engineering, 2020 Publication	<1 %
21	Yanfeng Chen, Weixin Huang, Donglin He, Yue Situ, Hong Huang. " Construction of Heterostructured g-C N /Ag/TiO Microspheres with Enhanced Photocatalysis Performance under Visible-Light Irradiation ", ACS Applied Materials & Interfaces, 2014 Publication	<1 %
22	Lawrence Munguti, Francis Dejene. "Influence of annealing temperature on structural, optical and photocatalytic properties of ZnO–TiO2 composites for application in dye removal in water", Nano-Structures & Nano-Objects, 2020 Publication	<1 %

23	businessdocbox.com Internet Source	<1%
24	koreascience.or.kr Internet Source	<1%
25	Bhavin Siritanaratkul, Shams T. A. Islam, Torsten Schubert, Cindy Kunze, Tobias Goris, Gabriele Diekert, Fraser A. Armstrong. "Selective, light-driven enzymatic dehalogenations of organic compounds", RSC Advances, 2016 Publication	<1%
26	core.ac.uk Internet Source	<1%
27	Sze-Mun Lam, Jin-Chung Sin, Ahmad Zuhairi Abdullah, Abdul Rahman Mohamed. " Photocatalytic TiO /Carbon Nanotube Nanocomposites for Environmental Applications: An Overview and Recent Developments ", Fullerenes, Nanotubes and Carbon Nanostructures, 2014 Publication	<1%
28	hdl.handle.net Internet Source	<1%
29	shareok.org Internet Source	<1%

30	Cui, Linfan, Tifeng Jiao, Qingrui Zhang, Jingxin Zhou, and Qiuming Peng. "Facile Preparation of Silver Halide Nanoparticles as Visible Light Photocatalysts", Nanomaterials and Nanotechnology, 2015. Publication	<1 %
31	Yen-Hua Chen, Kuo-Jui Tu. "Thickness Dependent on Photocatalytic Activity of Hematite Thin Films", International Journal of Photoenergy, 2012 Publication	<1 %
32	eprints.utm.my Internet Source	<1 %
33	espace.curtin.edu.au Internet Source	<1 %
34	"Perovskite Materials for Energy and Environmental Applications", Wiley, 2022 Publication	<1 %
35	Chitiphon Chuaicham, Sekar Karthikeyan, Jun Tae Song, Tatsumi Ishihara, Bunsho Ohtani, Keiko Sasaki. " Importance of ZnTiO Phase in ZnTi-Mixed Metal Oxide Photocatalysts Derived from Layered Double Hydroxide ", ACS Applied Materials & Interfaces, 2020 Publication	<1 %
36	Muhammad Shalahuddin Al Ja'farawy, Kusumandari, Agus Purwanto, Hendri	<1 %

Widiyandari. "Carbon quantum dots supported zinc oxide (ZnO/CQDs) efficient photocatalyst for organic pollutant degradation – A systematic review", Environmental Nanotechnology, Monitoring & Management, 2022
Publication

---

37 Sindhu, S.. "Structural, optical, physical and electrical properties of V"2O"5.SrO.B"2O"3 glasses", Spectrochimica Acta Part A: Molecular and Biomolecular Spectroscopy, 20060501
Publication

<1 %

---

38 pubs.acs.org
Internet Source

<1 %

---

39 www.nature.com
Internet Source

<1 %

---

40 Annette Madelene Dăncilă, Simona Căprărescu, Constantin Bobirică, Violeta Purcar et al. "Optimization of the Technological Parameters for Obtaining Zn-Ti Based Composites to Increase the Performance of H2S Removal from Syngas", Processes, 2020
Publication

<1 %

---

41 Zhenfeng Bian, Jian Zhu, Fenglei Cao, Yuning Huo, Yunfeng Lu, Hexing Li. "Solvothermal synthesis of well-defined TiO2 mesoporous

<1 %

nanotubes with enhanced photocatalytic activity", Chemical Communications, 2010
Publication

42 Rijuta G. Saratale, Hyun S. Noh, Ji Y. Song, Dong S. Kim. " Influence of parameters on the photocatalytic degradation of phenolic contaminants in wastewater using TiO /UV system ", Journal of Environmental Science and Health, Part A, 2014 <1%
Publication

43 Wang Ding, Suqin Liu, Zhen He. "One-step synthesis of graphitic carbon nitride nanosheets for efficient catalysis of phenol removal under visible light", Chinese Journal of Catalysis, 2017 <1%
Publication

Exclude quotes	Off	Exclude matches	Off
Exclude bibliography	On		

IOP2021_2

GRADEMARK REPORT

FINAL GRADE

/0

GENERAL COMMENTS

Instructor

PAGE 1

PAGE 2

PAGE 3

PAGE 4

PAGE 5

PAGE 6

PAGE 7

PAGE 8

PAGE 9

PAGE 10

PAGE 11